J. Fluid Mech. (1996), *vol.* 312, *pp.* 253–278

Nearly pure sorting waves and formation of bedload sheets

By GIOVANNI SEMINARA[1], MARCO COLOMBINI[1] AND GARY PARKER[2]

[1] Istituto di Idraulica, Facoltà di Ingegneria, Università di Genova, Italy

[2] St. Anthony Falls Hydraulics Laboratory, University of Minnesota, USA

(Received 17 October 1995 and in revised form 28 September 1995)

Bedload sheets are coherent migrating patterns of bed material recently observed both in flume studies and in field streams with beds of coarse sand and fine gravel. This newly recognized feature is inherently associated with the heterogeneous character of the sediment and consists of sorting waves with distinct coarse fronts only one or two coarse grains high.

The question of the formation of bedload sheets poses an interesting and peculiar stability problem for the grain size distribution. Sorting waves are essentially two-dimensional migrating perturbations associated with variations of this distribution. We show that their growth is strictly associated with grain sorting. In fact the latter gives rise to perturbations of bedload transport which drive small perturbations of bottom elevation the amplitude of which scales with grain size. The sorting wave also induces spatial variations of bottom roughness, and consequently alters the fluid motion, which conversely exerts a spatially varying stress on the bed. The feature of bedload sheets which allows them to be distinguished from dunes over beds with coarse sand or fine gravel is then the fact that sorting is the dominant effect controlling their growth, rather than being a relatively small perturbation of the mechanism which gives rise to dunes in the case of uniform sediment.

The requirement that perturbations should not alter the sediment budget leads to an integral condition which gives rise to an integro-differential mathematical problem. With the help of recently developed bedload relationships suitable for mixtures, as well as appropriate modelling of turbulent channel flow over a bed with spatially periodic perturbations of bottom elevation and roughness we are able to derive a general dispersion relation which can be readily solved in terms of undisturbed size densities in the form of sums of Dirac distributions.

Perturbations are found to be unstable within a range of wavenumbers depending on the relative roughness and Froude number. We show that when the effects of perturbations of bottom elevation are neglected the unstable region corresponds to the range of conditions where the bottom stress leads bottom roughness, a range distinct from that which characterizes the formation of dunes. This result is given a physical explanation which depends crucially on the deviation from equal mobility of different grain sizes in the surface layer. The effect of perturbations of bottom elevation is however not negligible when the bottom roughness is fairly large compared to depth. In the latter case perturbations of bottom elevation and of bottom roughness are equally important, and gravel sheets are not easily distinguished from small-amplitude dunes.

Comparison with the field observations of Whiting *et al.* (1985, 1988) is satisfactory insofar as the bedload sheet mode is unstable under the conditions of the experiments,

and the predicted wavelengths fall within the experimental range. The laboratory observations of Kuhnle & Southard (1988), on the other hand, appear to fall within a range of bottom roughness where the observed bedforms do not exhibit features unambiguously distinct from those of small-amplitude dunes.

---

1. Introduction

A distinct and fascinating feature of sediment set in motion in response to the action of a fluid in various natural environments (rivers, coastal areas, estuaries, deserts) is its tendency to exhibit a high level of spatial and temporal organization. This is displayed, for example, by the appearance of various types of bedforms, i.e. sandwaves characterized by a variety of spatial scales. Research developed mainly in the last two decades has provided a fairly consistent picture of the mechanisms underlying the formation of bedforms occurring in rivers. The common feature of the various processes is the inherent instability of flow and sediment transport in a straight channel to infinitesimal bottom perturbations. The latter give rise to perturbations of sediment transport rate which are generally out of phase with respect to bottom profile. As pointed out by Kennedy (1963) this phase lag is responsible for the growth of two-dimensional bedforms. The interested reader is referred to Engelund & Fredsøe (1982) and Seminara & Tubino (1989) for state of the art reviews related to 'small'-scale bedforms (ripples, dunes, antidunes) and 'large'-scale bedforms (bars) respectively.

In the present contribution we are concerned with a newly recognized type of organization of bed material recently detected both in flume studies (Iseya & Ikeda 1987; Kuhnle & Southard 1988) and in field observations in streams with beds of coarse sand and fine gravel (Whiting *et al.* 1985, 1988). This new feature is inherently associated with the heterogeneous character of sediments and is clearly described in Whiting *et al.* (1988): "... bed material was organized into waves with distinct coarse fronts. These fronts were only one or two coarse grains high but persisted with downstream migration of the wave as grains eroded from upstream were redeposited near the coarse leading edge. We have proposed the term "bedload sheets" to refer to these features (Whiting *et al.* 1985) whose overall morphology differs from that typical of ripples, dunes or other bed features previously described. A bedload sheet can be defined as a downstream migrating accumulation of bed material, coarsest at the leading edge, the length of which is much greater than the height, and the height of which is less than three coarse-grain diameters ..." (see figure 1).

The current interest in bedload sheets appears to have been sparked by the research of H. Ikeda and colleagues dating from 1984 and documented in the Japanese literature; see Iseya & Ikeda (1987) for reference to these.

An important phenomenon accompanying the formation and development of bedload sheets is the generation of "... cyclic pulses in sediment transport rates that vary up to a factor of order 10 ..." (Whiting *et al.* 1988). Transport rates reach a maximum soon after the passage of the coarse front. Understanding the mechanics of this new type of bedform may thus provide the basis to explain one reason for the commonly observed large temporal and spatial variations in the bedload transport rate of rivers.

Bedload sheets were observed by Whiting *et al.* (1988) at two field sites. In one case they formed on the stoss side of dunes, the wavelength of sheets being somewhat

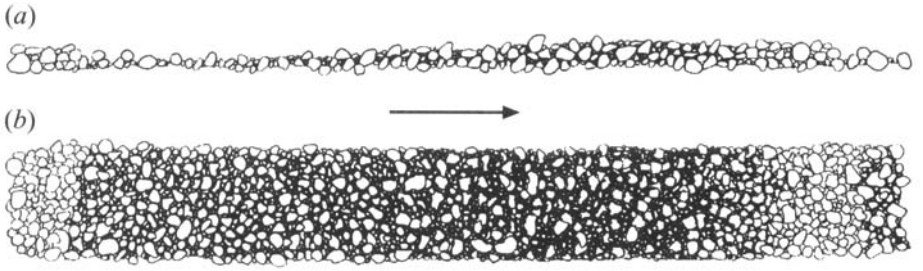

FIGURE 1. Sketch of bedload sheets as reported by Whiting *et al.* (1988): (*a*) side and (*b*) plan view.

smaller than the wavelength of coexisting dunes. Kuhnle & Southard's (1988) data, on the other hand, refer to laboratory observations where dunes were not present.

Let us then ask the first fundamental question: why do bedload sheets form? Whiting *et al.* (1988) hypothesize that they "... result primarily from an inherent instability associated with the interaction of multiple size fractions during bedload transport of poorly sorted sediment ...". Quite recently Tsujimoto (1989) has elaborated upon the above idea by attempting a stability analysis of bedload transport of a sediment mixture composed of two size fractions, one in the gravel range and the other in the sand range. Tsujimoto's (1989) basic idea is that the mechanism underlying the process of sheet formation would be the selective and non-equilibrium properties of bedload transport, in a similar fashion to that proposed by Nakagawa & Tsujimoto (1980) to explain dune formation in rivers, the distinct feature of the sheet case being the heterogeneous character of the sediment. Tsujimoto's (1989) treatment of sediment transport in terms of pickup and step length offers a viable alternative to the Exner-type formulation presented here. The flow model, however, which is based on a direct application of the Manning–Strickler equation to disequilibrium flow, would seem to be a gross and unnecessary oversimplification that might obscure the true nature of the phenomenon.

In the present contribution we attempt to provide a somewhat different explanation of the mechanism of sheet formation. We consider the motion of a sediment mixture characterized by some continuous probability density function F for grain size ϕ (in the sedimentological scale such that the dimensional grain diameter D^* equals $2^{-\phi}$ mm) uniformly distributed in space and time as appropriate to uniform flow conditions. We then investigate the stability of such a distribution to linear perturbations both in space and time in the form of growing and travelling waves, but constrained so as to satisfy the integral condition

$$\int_{-\infty}^{\infty} F(\phi)\mathrm{d}\phi = 1. \tag{1.1}$$

The occurrence of such perturbations may be either associated with the formation of bedforms such as dunes or with the development of bedload sheets. Thus the need arises for a theory able to distinguish between the mechanisms causing the phenomenon.

Indeed the basic question which needs to be answered preliminarily is the following: does the dynamics of a sediment mixture allow for the growth and propagation of pure sorting waves? In other words are regular periodic perturbations of the grain size distribution able to form and migrate on a strictly flat bottom? It will be shown below that the answer to this question is negative. However it will be seen that 'nearly

pure' sorting waves are indeed possible, the qualification 'nearly' simply meaning that small variations of bottom amplitude which scale with grain size rather than with flow depth (as in the case of dunes) must be allowed.

Under such conditions what is, then, the mechanism which controls the growth of sorting waves?

The basic idea is as follows: periodic perturbations of the average grain size associated with the formation of bedload sheets are felt by the fluid as periodic perturbations of bottom roughness. It follows that bottom stress is also subject to periodic variations which may lag behind or lead ahead of the corresponding perturbations of average grain size depending on the perturbation wavenumber. Sorting also drives spatial perturbations of the bedload transport rate which give rise to perturbations of bottom elevation. The requirement of sediment continuity for each size along with the integral condition (1.1) then leads to a dispersion relation which shows that perturbations do indeed grow within a range of wavenumbers, depending on the relative roughness and on the Froude number of the flow, provided the mobilities of different grain sizes in the surface layer are unequal. This is shown analytically for the case of small standard deviations of the mixture and mixtures composed of two sizes. The case of arbitrary size distribution is then analysed.

The interest and novelty of the analysis proposed in the present paper appears to be of more general significance. Indeed the effect of sorting on all river bedforms can be incorporated into the classical approaches following ideas similar those presented herein.

The development of the above analysis has been made possible by recent achievements in modelling of bedload transport of sediment mixtures. In the next section the main results of these latter investigations will be reviewed in the context of the formulation of the present problem. The perturbations of bottom stress induced by a spatially varying bottom elevation and roughness are derived in §3. Section 4 is devoted to the stability analysis. The instructive case of a mixture characterized by small standard deviation is analysed in §5. Section 6 is devoted to results and comparison with experimental observations, along with some conclusions.

2. Formulation of the problem

Let us consider uniform turbulent free surface flow of an incompressible fluid of density ρ in a wide straight channel and refer to Cartesian coordinates (x^*, y^*), the x^* axis being aligned with the uniform flow direction. Hereafter a star superscript will denote dimensional quantities. We denote by H_0^*, U_0^*, Fr, S the uniform values of flow depth, average speed, Froude number and slope of the channel respectively.

We assume the channel bottom to be cohesionless, and denote by $F(\phi; x^*, t^*)$ the probability density function describing the distribution of grain sizes available for transport. Sediment available for transport lies in a surface layer, called the active layer (Hirano 1971), which is known to be coarser than the substrate at low flow rate, a phenomenon called 'mobile armoring'. The thickness L_a^* of the active layer under flat bed conditions is usually assumed to scale with D_{90}^*, i.e. the grain size such that 90% of the sample is finer.

In general, as indicated above, F may depend both on space and time. We denote by $F_0(\phi)$ the distribution associated with the basic uniform flow. We wish to investigate the development of perturbed configurations, and thus denote by $f(x^*, t^*)$ the perturbation of the grain size probability density function. The latter perturbations drive flow perturbations which, as usual in bedform instability problems, develop much

faster than the bottom. Hence the flow can be assumed to adapt instantaneously to any variation of grain size distribution. This assumption of quasi-steady flow implies that the flow equations may be decoupled from the sediment continuity equation. Flow perturbations determine the distribution of bottom shear stress, which in turn controls bedload transport of each size fraction.

The first ingredient with which to tackle the above problem is the development of an appropriate dynamic equation for bedload transport of a mixture.

Equilibrium transport formulas for mixtures have been the subject of several investigations in recent years. One of the present authors has recently (Parker 1992) reviewed this topic. The reader is referred to that paper for details. Here we simply recall the main conclusions which can be reached on the basis of most recent research.

It has long been recognized since the work of Einstein (1950) and Egiazaroff (1965) that the dynamics of a sediment mixture is characterized by a so-called 'hiding' effect whereby fluid drag acts more intensely on coarser grains, which typically protrude more into the turbulent boundary layer than finer grains. Hiding counteracts the opposing effect of gravity, which makes finer grains more mobile than the heavier coarse grains.

In order to quantify the above effects it is convenient to express the volume bedload discharge per unit width q^* for a uniform sediment with relative density s subject to a uniform bottom stress τ_0^* in the form

$$q = \tau_*^{3/2} G(\tau_*), \tag{2.1}$$

where

$$q = \frac{q^*}{[(s-1)gD^{*3}]^{1/2}}, \tag{2.2}$$

$$\tau_* = \frac{\tau_0^*}{\rho(s-1)gD^*}. \tag{2.3}$$

The dimensionless quantity τ_* is known as the Shields stress. If G were constant the bedload discharge would be independent of sediment size, as grain diameter is present both in the scaling of q^* and of $\tau_0^{*3/2}$ in identical form. However for uniform sediments G is found to be a rapidly increasing function of τ_*. This is particularly true in the neighbourhood of the critical condition for sediment motion. The simplest generalization of (2.1) for a mixture would be of the form

$$q_\phi = \tau_*^{3/2} G[\tau_*(\phi)] F(\phi), \tag{2.4}$$

where $q_\phi \mathrm{d}\phi$ is the volumetric bed load discharge per unit width of grains in the size range $\phi, \phi + \mathrm{d}\phi$, $\tau_*(\phi)$ is the Shields stress associated with grain size ϕ, and G is a function taken to be identical to the function obtained for uniform sediment. Such a generalization would, however, be inappropriate as it does not account for hiding and ensures an extremely strong bias towards fine material in the transported bedload. Indeed the size density of the transported bed load material $F_T(\phi)$ reads

$$F_T(\phi) = \frac{G[\tau_*(\phi)]F(\phi)}{\int_{-\infty}^{\infty} G[\tau_*(\phi)]F(\phi)\mathrm{d}\phi}. \tag{2.5}$$

It is seen that G plays the role of a weight function such that larger values of ϕ, i.e. finer material, lead to larger values of F_T.

In order to overcome the above difficulty it has been suggested by various authors

(Ashida & Michiue 1972; Proffitt & Sutherland 1983; White & Day 1982; Samaga, Ranga Raju & Garde 1986; Ribberink 1987; Parker 1990) that the function G should be modified through the inclusion of a weight function g_h able to mitigate the bias toward fine material in the bedload relation.

In Parker (1990) the following form for the function G is proposed:

$$G(\zeta) = 0.00218 \begin{cases} 5474(1 - 0.853/\zeta)^{4.5}, & \zeta > 1.59 \\ \exp[14.2(\zeta - 1) - 9.28(\zeta - 1)^2], & 1 < \zeta < 1.59 \\ \zeta^{14.2}, & \zeta < 1, \end{cases} \tag{2.6}$$

where ζ is a dummy parameter.

Denoting by D_g^* the geometric mean size, Parker (1992) suggests for ζ the general form

$$\zeta = \frac{\tau_{*g}}{\tau_{*r}} \frac{D_g^*}{D^*} g_h \left(\frac{D^*}{D_g^*} \right), \tag{2.7}$$

where τ_{*g} is Shields stress based on the geometric mean diameter D_g^* and τ_{*r} is a reference Shields stress. It follows easily from (2.7) that if the approximation of substrate-based 'equal mobility' of Parker & Klingeman. (1982) were to prevail for surface material as well then the hiding function g_h must be given by $g_h = D^*/D_g^*$.

Parker (1990) used the concept of (2.7) to develop the slightly more general form

$$\zeta = \omega \frac{\tau_{*g}}{\tau_{*r}} \left(\frac{D^*}{D_g^*} \right)^{-\beta}, \tag{2.8}$$

where ω is a straining function of the form

$$\omega = \omega \left(\sigma, \frac{\tau_{*g}}{\tau_{*r}} \right) \tag{2.9}$$

and

$$\sigma^2 = \int_{-\infty}^{\infty} (\phi - \phi_g)^2 F \mathrm{d}\phi, \qquad \phi_g = \int_{-\infty}^{\infty} F \phi \mathrm{d}\phi. \tag{2.10a,b}$$

The parameter β in (2.8) takes the value 0.095, corresponding to a hiding function of the form $g_h = (D^*/D_g^*)^{0.905}$. The fact that $\beta > 0$ means that the bedload size distribution is systematically finer than that of the surface material. The reference Shields stress τ_{*r} takes the value 0.0386. Note that the straining function ω explicitly accounts for the effect of the standard deviation σ of the surface grain size distribution on the transport rate. A form for this straining function has been proposed by Parker (1990) based on field observations.

The appropriate generalization of (2.4) is then

$$q_g = q_u F, \qquad q_u = \tau_{*g}^{3/2} G(\zeta) \tag{2.11a,b}$$

where q_g corresponds to q_ϕ, but is scaled using D_g^* rather than D^* as reference length and ζ is defined by (2.8).

The basic equation governing the bedload sheet problem is a statement of mass balance which must be imposed upon each size fraction. Since bedload sheets may be considered to result from a rearrangement of the material present in the active layer such that the bottom develops only minimal topography, we may neglect interaction between the substrate and the active layer. Denoting by η^* bottom elevation and by p the porosity of the mixture, a grain-size-specific statement for mass balance (reduced to a volume balance if sediment density is uniform) takes the dimensional form (see

Parker 1992)

$$(1-p)(F\eta^*_{,t^*} + L^*_a F_{,t^*}) = -(q^*_u F)_{,x^*}. \tag{2.12}$$

It is convenient to reduce (2.12) to dimensionless form by defining

$$q_u = \frac{q^*_u}{[(s-1)gD^{*3}_{go}]^{1/2}}, \tag{2.13}$$

$$x = \frac{x^*}{H^*_0}, \tag{2.14}$$

$$(\eta, L_a) = \frac{(\eta^*, L^*_a)}{D^*_{go}}, \tag{2.15}$$

$$t = \frac{[(s-1)gD^{*3}_{go}]^{1/2}}{(1-p)H^*_0 D^*_{go}} t, \tag{2.16}$$

where D^*_{go} denote the median diameter of the surface layer under uniform flow conditions. Sediment continuity then reads

$$F\eta_{,t} + L_a F_{,t} = -(q_u F)_{,x}. \tag{2.17}$$

Notice that the scaling (2.15) is appropriate to the case of bedload sheets the amplitude of which scales with the grain size rather than on the flow depth as in the case of dunes.

Equation (2.17) must be coupled with a dynamic equation for sediment motion. The simplest assumption at this stage is to assume that bedload sheets constitute a quasi-equilibrium configuration such that bed load discharge for each size is determined only by the local value of Shields stress. In this case the appropriate dynamic equation simply reads

$$q_u = \tau^{3/2}_{*g} G(\zeta), \qquad \zeta = T\left(\frac{D^*}{D^*_g}\right)^{-\beta} \omega, \qquad T = \frac{\tau_{*g}}{\tau_{*r}} \frac{D^*_{go}}{D^*_g}, \tag{2.18a–c}$$

where τ_{*g} is the Shields stress based on the undisturbed value of the geometric mean size D^*_{go}. That is,

$$\tau_{*g} = \frac{[(\boldsymbol{T}\cdot\hat{\boldsymbol{n}})\cdot\hat{\boldsymbol{t}}]_\eta}{\rho(s-1)gD^*_{go}}, \tag{2.19}$$

where $\boldsymbol{T}$ is the stress tensor associated with the motion of the fluid evaluated at the bottom, and $\hat{\boldsymbol{n}}$ and $\hat{\boldsymbol{t}}$ are the unit vectors normal and tangential to the bottom respectively.

The straining parameter ω can now be cast as a function of the form

$$\omega = \omega(\sigma, T). \tag{2.20}$$

Finally, the thickness L^*_a of the active layer is taken to be proportional to a typical coarse grain size D^*_σ defined as

$$D^*_\sigma = D^*_g 2^\sigma. \tag{2.21}$$

Here D^*_σ becomes identical to D^*_{84} in the case of a lognormal distribution. In general D^*_σ can be expected to be close to D^*_{90}. Hence we write

$$L_a = n_a \frac{D^*_g}{D^*_{go}} 2^\sigma, \tag{2.22}$$

where n_a is an order-one coefficient.

We point out that the quasi-equilibrium assumption is a convenient one when the spatial variations of Shields stress are very slow. When the wavelength of bedload sheets is of the order of one flow depth, however, the above assumption might be too restrictive. Tsujimoto's (1989) analysis of sediment mass balance might provide a less restrictive formulation, although the flow model offered there would require amendment to one closer to the one presented below.

The mathematical problem governing sediment motion is, then, formulated by (2.17)–(2.22) along with the integral condition (1.1). The latter problem is coupled with that governing the motion of the fluid in a channel characterized by spatially varying roughness and bottom elevation. This topic will be covered in the following section.

3. Flow field in a channel with small-amplitude periodic roughness perturbations

We consider a viscous incompressible fluid flowing in an infinitely wide channel with a bed characterized by a variable roughness. More precisely we assume the roughness height k_r to be proportional to D_σ^* as defined by (2.21) with a value of the constant of proportionality usually ranging between 2 and 3.5 for gravel bed rivers.

The question of how quickly a turbulent boundary layer responds to a variation of roughness has been addressed by numerous researchers. Jacobs (1939), Townsend (1961, 1965), Antonia & Luxton (1971, 1972), Nezu *et al.* (1990) and Tsujimoto, Cardoso & Saito (1990) have analysed both theoretically and experimentally the problem in the case of a step-like abrupt change of roughness in boundary layers and channel flows. Both the theoretical work and the experimental results show that flow perturbations are confined within an inner boundary layer, the outer layer remaining practically unaltered except for a streamline displacement effect. The latter finding applies to the case of zero-pressure-gradient boundary layers. In this case a step-like change of roughness induces a perturbation layer the thickness of which increases downstream, and a transition occurs from the self-preserving structure of the boundary layer upstream to a new self-preserving structure downstream. Whereas all theoretical treatments assume the persistence of a near-wall equilibrium layer in the transitional regime, the experimental findings of Antonia & Luxton (1972) suggest that deviations from equilibrium occur due to a non-negligible effect of longitudinal advection and transverse turbulent diffusion of longitudinal momentum. As a result the mixing length distribution in the inner layer is still linear in the vertical coordinate, but the proportionality constant is smaller (larger) than the Kármán constant for a smooth to rough (rough to smooth) variation of roughness.

All the above results are based on experiments performed on a single type of roughness. No information is available on the effect of changing the amplitude of the latter nor are the authors aware of experiments which involve different spatial distributions of roughness.

In the present problem roughness variations are taken to be spatially periodic and characterized by infinitesimal amplitude. We will take advantage of the above assumptions by hypothesizing that deviations from equilibrium in the inner layer are also small and may be described by linearized forms of the appropriate conservation equations and of the classical closure assumptions.

Let us then refer to a Cartesian coordinate system (x^*, y^*) such as the one sketched in figure 2 and denote by (U^*, V^*) the corresponding local velocity vector averaged over turbulence. The three curves $y^* = y_s^*, y^* = y_b^*$ and $y^* = y_r^*$ identify the free

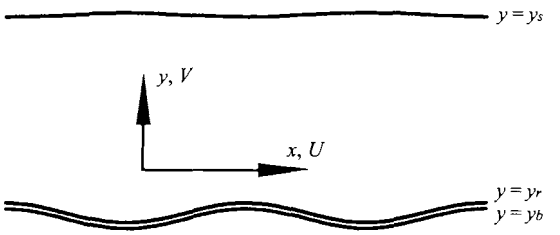

FIGURE 2. Sketch of the channel and notation.

and bottom surface and the reference level respectively. The reference level is defined as the conventional offset level at which the mean velocity essentially vanishes. The distance between the bed and the reference level is assumed, as for a uniform flow, to be proportional to the local value of the above-mentioned roughness height.

The steady Reynolds equations in dimensionless form then read

$$UU_{,x} + VU_{,y} = -P_{,x} + T_{xx,x} + T_{xy,y} + 1, \tag{3.1}$$

$$UV_{,x} + VV_{,y} = -P_{,y} + T_{xy,x} + T_{yy,y}, \tag{3.2}$$

$$U_{,x} + V_{,y} = 0, \tag{3.3}$$

where P is the mean dynamic pressure and T_{ij} is the Reynolds stress tensor. Variables have been made dimensionless using the friction velocity and depth of the unperturbed uniform flow and the fluid density.

The kinematic and dynamic boundary conditions to be associated with (3.1)–(3.3) read

$$\boldsymbol{U} \cdot \boldsymbol{e}_{tb} = 0 \quad \text{(dynamic)}, \tag{3.4}$$

$$\boldsymbol{U} \cdot \boldsymbol{e}_{nb} = 0 \quad \text{(kinematic)}, \tag{3.5}$$

at the bottom ($y = y_r$), while at the free surface ($y = y_s$) we have

$$\boldsymbol{e}_{ts} \cdot \boldsymbol{T} \cdot \boldsymbol{e}_{ns} = 0 \quad \text{(dynamic)}, \tag{3.6}$$

$$\boldsymbol{e}_{ns} \cdot \boldsymbol{T} \cdot \boldsymbol{e}_{ns} = 0 \quad \text{(dynamic)}, \tag{3.7}$$

$$\boldsymbol{U} \cdot \boldsymbol{e}_{ns} = 0 \quad \text{(kinematic)}, \tag{3.8}$$

where $\boldsymbol{U}$ is the two-dimensional velocity vector (U, V), $\boldsymbol{T}$ is the two-dimensional Reynolds stress tensor and $\boldsymbol{e}_{tb}, \boldsymbol{e}_{ts}, \boldsymbol{e}_{nb}$, and $\boldsymbol{e}_{ns}$ are the unit vectors tangential and normal to bottom and free surface respectively.

In order to close the above formulation we employ a Boussinesq-type assumption which reads

$$T_{ij} = \nu_T (U_{,j} + V_{,i}), \tag{3.9}$$

with $i = x, y$, $j = x, y$ and ν_T dimensionless eddy viscosity. Furthermore we assume weak perturbations of bottom roughness, and accordingly use a mixing length structure for ν_T in the form

$$\nu_T = \ell^2 \frac{\partial U}{\partial y}, \tag{3.10}$$

where ℓ is a dimensionless mixing length given by

$$\ell = \kappa (y - y_b) \left(\frac{y_s - y}{H} \right)^{1/2}, \qquad H = y_s - y_r. \tag{3.11}$$

In the above H is the dimensionless local flow depth and κ is the Kármán constant.

We point out that results obtained in the absence of roughness variation through the above simple closure scheme have been compared with those derived by means of the more complete one-equation closure model employed by Richards (1980). The latter model expresses eddy viscosity in terms of the turbulent kinetic energy, for which an appropriate balance is imposed between production, dissipation, advection and diffusion. Results of the two models were found to be so similar both qualitatively and quantitatively that it seemed convenient to minimize the numerical effort by using the above local assumptions. It will become apparent below that the mixing length assumption (3.10) allows for small perturbations with respect to the unperturbed configuration.

It is convenient for numerical purposes to employ the following transformation of variables:

$$\chi = \frac{y - y_r(\xi)}{y_s(\xi) - y_r(\xi)}, \qquad \xi = x. \tag{3.12}$$

Furthermore we stipulate that

$$y_r - y_b = R = mk_r, \tag{3.13}$$

where m is a constant that has traditionally been set equal to $\frac{1}{30}$ based on the logarithmic law for rough flow.

We now assume the following representation of the flow field:

$$\begin{aligned}(U, V, P, H, \ell, \nu_T, R, y_b) = (U_0, 0, P_0, 1, \ell_0, \nu_{To}, R_0, 0)\\ +\epsilon[(U_1, V_1, P_1, H_1, \ell_1, \nu_{T1}, R_0 r, e)\exp \mathrm{i}\alpha\xi + \text{c.c.}] + O(\epsilon^2),\end{aligned} \tag{3.14}$$

with the parameter ϵ chosen to be small in accordance with the assumption of weak perturbations of the uniform configuration. Note here that e denotes the perturbation of bed elevation and r denotes a normalized perturbation of bed roughness. These two parameters play an important role in the succeeding analysis.

The above expansion can then be substituted into the governing equations, boundary conditions and closure assumptions to obtain a sequence of problems at the various orders of approximation in the small parameter ϵ. We skip the details of the latter procedure, which is tedious but standard, and simply show the main results.

$O(\epsilon^0)$

At leading order we recover the equilibrium uniform solution written in terms of the transformed coordinates ξ and χ. More precisely we obtain the following, where the primes denote differentiation with respect to χ:

$$\nu_{T0}U_0'' + \nu_{T0}'U_0' = -1, \qquad P_0' = 0, \tag{3.15a,b}$$

$$U_0|_{\chi=0} = 0, \qquad \nu_{T0}U_0'|_{\chi=1} = 0, \qquad P_0|_{\chi=1} = 0, \tag{3.16a–c}$$

where

$$\nu_{T0} = \ell_0^2 U_0', \qquad \ell_0 = k(\chi + R_0)(1-\chi)^{1/2}. \tag{3.17a,b}$$

In the above equations and in the following, we have neglected $R_0 = mk_{ro}$ with respect to 1, i.e. one thirtieth of the roughness height is neglected compared to the depth, an assumption which can be expected to be valid for all but extremely shallow flows. The above system immediately integrates to yield

$$U_0 = \frac{1}{\kappa}\ln\left[\frac{\chi + R_0}{R_0}\right], \qquad P_0 = 0, \tag{3.18a,b}$$

i.e. the classical rough logarithmic law.

$O(\epsilon^1)$

It is convenient to express the $O(\epsilon^1)$ solution in the form

$$(U_1, H_1) = (u(\chi), h), \qquad (V_1, P_1) = \mathrm{i}\alpha(v(\chi), p(\chi)), \tag{3.19a,b}$$

so that the differential equations governing the unknown functions $u(\chi), v(\chi), p(\chi), h(\chi)$ can be written as

$$\mathbf{L}\boldsymbol{Z} = \boldsymbol{A}\boldsymbol{f}, \tag{3.20}$$

where

$$\boldsymbol{Z} = \begin{pmatrix} u \\ v \\ p \end{pmatrix}, \qquad \boldsymbol{f} = \begin{pmatrix} h \\ e \\ r \end{pmatrix}, \tag{3.21}$$

while the linear differential operator $\mathbf{L}$ and the matrix $\boldsymbol{A}$ are given in Appendix A.

Imposing the linearized boundary conditions (provided by (3.4)–(3.8)), the differential problem (3.20) is readily solved numerically by shooting techniques. Its solution can be written as

$$\boldsymbol{Z} = \boldsymbol{Z}_{hom} + \boldsymbol{Z}_h h + \boldsymbol{Z}_e e + \boldsymbol{Z}_r r, \tag{3.22}$$

with the subscript *hom* referring to the homogeneous part of the above differential system, while the subscripts h, e, r refer to particular solution of the complete system. The amplitude of depth variation h can be expressed in term of e and r to give the relative amplitude of free surface undulations.

Once the solution is available the bottom stress can be evaluated in the dimensionless form

$$\tau = \nu_T(U_{,y} + V_{,x})|_{y=y_r}. \tag{3.23}$$

Scaling τ in Shields form one can eventually derive the following relationship for Shields stress:

$$\tau_{*g} = \tau_{*go}\{1 + \epsilon[\tau_{*g1} \exp \mathrm{i}\alpha\xi + \text{c.c.}]\}, \tag{3.24}$$

where τ_{*go} is the unperturbed Shields stress and τ_{*g1} is the correction associated with the perturbation of bottom amplitude and roughness.

Needless to say τ_{*g1} is a complex number the imaginary part of which controls the phase lag of τ_{*g} with respect to D_g. After some algebra τ_{*g1} may be related to the flow field as follows:

$$\tau_{*g1} = \left[2\left.\frac{u'}{U_0'}\right|_{\chi=0} - 2h\right]_e e + \left[2\left.\frac{u'}{U_0'}\right|_{\chi=0} - 2h + 2\right]_r r = t_e e + t_r r, \tag{3.25}$$

where again t_e and t_r are in general complex, serving to quantify the effects of variation in bed elevation and roughness, respectively, on the Shields stress.

4. Bedload sheet instability: formulation

We now investigate the development of bedload sheets, i.e. perturbations of the grain size distribution which drive perturbations of bottom elevation.

Let us assume

$$(F, \phi_g, \sigma) = (F_0(\phi), \phi_{go}, \sigma_0) + \epsilon\left[(\mathscr{F}(t, \phi), \varphi_g(t), \sigma_0\sigma_1(t)) \exp \mathrm{i}\alpha x + \text{c.c.}\right], \tag{4.1}$$

$$\eta = \eta_0 + \epsilon[e(t) \exp \mathrm{i}\alpha x + \text{c.c.}], \tag{4.2}$$

where

$$\phi_{go} = \int_{-\infty}^{\infty} F_0 \phi \mathrm{d}\phi, \qquad \sigma_0^2 = \int_{-\infty}^{\infty} (\phi - \phi_{go})^2 F_0 \mathrm{d}\phi, \tag{4.3a,b}$$

$$\varphi_g = \int_{-\infty}^{\infty} \mathscr{F} \phi \mathrm{d}\phi, \qquad \sigma_1 = \frac{1}{2\sigma_0^2} \int_{-\infty}^{\infty} (\phi - \phi_{go})^2 \mathscr{F} \mathrm{d}\phi. \tag{4.4a,b}$$

Here φ_g characterizes the perturbation of mean surface grain size and σ_1 characterizes the perturbation of surface standard deviation.

According to (3.13) and the previously introduced assumption that k_r is proportional to D_σ^*, it is readily found that

$$r = \ln(2)(-\varphi_g + \sigma_0 \sigma_1). \tag{4.5}$$

Equations (3.24), (3.25) and (4.5) can now be combined to yield

$$\tau_{*g} = \tau_{*go}\{1 + \epsilon[(t_\varphi \varphi_g + t_\sigma \sigma_0 \sigma_1 + t_e e) \exp \mathrm{i}\alpha x + \text{c.c.}]\}, \tag{4.6}$$

where $t_\sigma = -t_\varphi = t_r \ln 2$.

The above expansion describes the physical mechanism whereby perturbations of F are felt by the flow field as perturbations of local roughness, thus inducing a secondary flow which in turn gives rise to perturbations of bottom stress. Further contributions to the latter are also induced by the small perturbations of bottom amplitude needed for mass conservation of the sediment mixture to be satisfied.

The argument ζ of the function G (see 2.18b) can be written as

$$\zeta = \omega 2^{\beta(\phi - \phi_g) + (\phi_g - \phi_{go})} \frac{\tau_{*g}}{\tau_{*r}}, \tag{4.7}$$

and expanded in the form

$$\zeta = \zeta_0\{1 + \epsilon[(\zeta_{1\varphi} \varphi_g + \zeta_{1\sigma} \sigma_0 \sigma_1 + \zeta_{1e} e) \exp \mathrm{i}\alpha x + \text{c.c.}]\}, \tag{4.8}$$

leading to the following relationships for the coefficients at $O(\epsilon)$:

$$\zeta_{1\varphi} = \ln 2(1 - \beta + \omega_T) + t_\varphi(1 + \omega_T), \tag{4.9}$$

$$\zeta_{1\sigma} = t_\sigma(1 + \omega_T) + \omega_\sigma, \tag{4.10}$$

$$\zeta_{1e} = t_e(1 + \omega_T), \tag{4.11}$$

where

$$\omega_T = \left[\frac{T}{\omega} \frac{\partial \omega}{\partial T}\right]_{T=T_0, \sigma=\sigma_0}, \qquad \omega_\sigma = \left[\frac{1}{\omega} \frac{\partial \omega}{\partial \sigma}\right]_{T=T_0, \sigma=\sigma_0}. \tag{4.12a,b}$$

Combining (2.18) with (4.6) and (4.8) we can finally expand the bedload discharge per unit width as

$$q_u = q_{uo}\{1 + \epsilon[(q_\varphi \varphi_g + q_\sigma \sigma_0 \sigma_1 + q_e e) \exp \mathrm{i}\alpha x + \text{c.c.}]\}, \tag{4.13}$$

with the following relations for the basic state:

$$q_{uo} = \tau_{*go}^{3/2} G(\zeta_0), \tag{4.14}$$

$$\zeta_0 = \omega_0 2^{\beta(\phi - \phi_{go})} T_0, \tag{4.15}$$

where

$$T_0 = \frac{\tau_{*go}}{\tau_{*r}}, \qquad \omega_0 = \omega(T_0, \sigma_0). \tag{4.16a,b}$$

The complex coefficients q_φ, q_σ and q_e represent the perturbations of the bedload

discharge per unit width due to variations of the mean and variance of the grain size distribution (φ_g, σ_1) and to the perturbation of bottom elevation (e). They are, respectively,

$$q_\varphi = \Gamma \zeta_{1\varphi} \qquad q_\sigma = \tfrac{3}{2} t_\sigma + \Gamma \zeta_{1\sigma}, \qquad q_e = \tfrac{3}{2} t_e + \Gamma \zeta_{1e}, \tag{4.17a–c}$$

where the parameter Γ is defined as

$$\Gamma = \left[\frac{\zeta}{G(\zeta)} \frac{\mathrm{d}G}{\mathrm{d}\zeta} \right]_{\zeta=\zeta_0}. \tag{4.18}$$

Before feeding the expansions (4.1), (4.2), (4.6), (4.8), (4.13) into the sediment continuity equation (2.17) we must also expand the thickness of the active layer L_a which is taken to be proportional to D_σ^*. We will need only the unperturbed value of L_a, namely

$$L_{ao} = n_a 2^{\sigma_0}. \tag{4.19}$$

Hence, at order ϵ, (2.17) reads

$$F_0 e_{,t} + L_{ao} \mathscr{F}_{,t} = -\mathrm{i}\alpha q_{uo} \left\{ F_0 \left[q_\varphi \varphi_g(t) + q_\sigma \sigma_0 \sigma_1(t) + q_e e(t) \right] + \mathscr{F}(\phi, t) \right\}. \tag{4.20}$$

If bedload sheets are to be distinguished from dunes, which are associated primarily with the bed perturbation e, then the mean grain size perturbation φ_g and the perturbation of the standard deviation σ_1 must play a crucial role as regards the former.

Let us now impose on (4.20) the conditions

$$\int_{-\infty}^{\infty} F_0 \mathrm{d}\phi = 1, \qquad \int_{-\infty}^{\infty} \mathscr{F} \mathrm{d}\phi = 0, \tag{4.21a,b}$$

which follow from (1.1). We are led to a system of two integro-differential equations for the unknown functions $e(t), \mathscr{F}(t, \phi)$

$$\begin{aligned} L_{ao} \mathscr{F}_{,t} = &-\mathrm{i}\alpha \left\{ F_0 \left[\left(q_{uo} q_\varphi - \overline{q_{uo} q_\varphi} \right) \varphi_g + \left(q_{uo} q_\sigma - \overline{q_{uo} q_\sigma} \right) \sigma_0 \sigma_1 + \left(q_{uo} q_e - \overline{q_{uo} q_e} \right) e \right] \right\} \\ &- \mathrm{i}\alpha \left\{ q_{uo} \mathscr{F} - F_0 \int_{-\infty}^{\infty} q_{uo} \mathscr{F} \mathrm{d}\phi \right\}, \end{aligned} \tag{4.22a}$$

$$e_{,t} = -\mathrm{i}\alpha \left\{ \overline{q_{uo} q_\varphi} \varphi_g + \overline{q_{uo} q_\sigma} \sigma_0 \sigma_1 + \overline{q_{uo} q_e} e + \int_{-\infty}^{\infty} q_{uo} \mathscr{F} \mathrm{d}\phi \right\}, \tag{4.22b}$$

where the overbar is defined as follows: let $\mathscr{A}$ be a generic function of ϕ, then

$$\overline{\mathscr{A}} = \int_{-\infty}^{\infty} \mathscr{A} F_0 \mathrm{d}\phi. \tag{4.23}$$

The solution of (4.22) can be written in the form

$$(e, \mathscr{F}) = (\hat{e}, f) \exp(-\mathrm{i}\alpha c t), \tag{4.24}$$

where $\hat{e}$ and $f(\phi)$ are solutions of a system of two integral equations obtained by substituting from (4.24) into (4.22).

At this point the solution procedure can be greatly simplified by approximating the continuous size distributions for $F_0(\phi)$ and $f(\phi)$ by a series of n steps associated with sizes $\phi_i, i = 1, 2, \ldots, n$, as shown in figure 3. The density function F_0 for such a mixture may be written in the form

$$F_0 = \sum_{i=1}^{n} F_{oi} \delta(\phi - \phi_i), \tag{4.25}$$

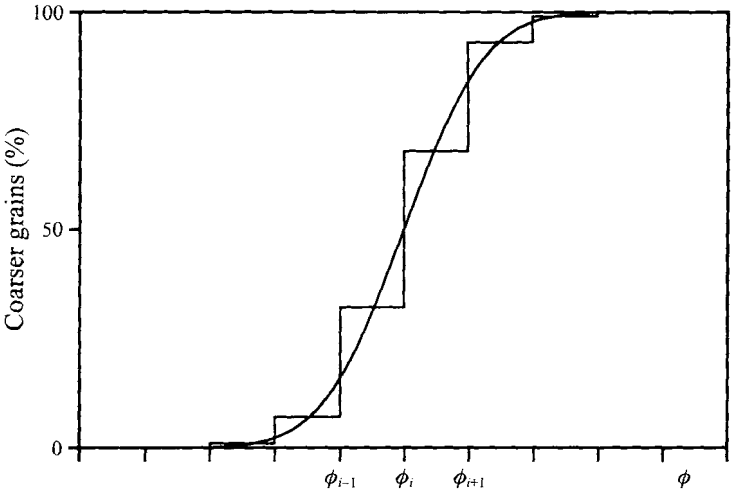

FIGURE 3. Schematic of continuous and discrete cumulative grain size distributions.

where $\delta(\phi - \phi_i)$ is a Dirac function centred at ϕ_i. The condition (4.21a) then requires that

$$\sum_{i=1}^{n} F_{oi} = 1. \tag{4.26}$$

Similarly, recalling (4.21b) we can express the amplitude of the perturbation f in the form

$$f = \sum_{i=1}^{n} f_i \delta(\phi - \phi_i), \tag{4.27}$$

with

$$\sum_{i=1}^{n} f_i(t) = 0. \tag{4.28}$$

From (4.23) it finally follows that

$$\overline{\mathscr{A}} = \int_{-\infty}^{\infty} \mathscr{A} F_0 \mathrm{d}\phi = \int_{-\infty}^{\infty} \mathscr{A} F_{oi} \delta(\phi - \phi_i) \mathrm{d}\phi = \sum_{i=1}^{n} \mathscr{A}_i F_{oi}, \tag{4.29}$$

where $\mathscr{A}_i$ is the value of the function $\mathscr{A}$ evaluated at $\phi = \phi_i$.

Recalling (4.28) we derive a system of n equations in the n unknowns $f_i(t)(i = 1, 2, \ldots, n-1)$ and $\hat{e}$. Integrating (4.22a) from ϕ_i^- to $\phi_i^+(i = 1, 2, \ldots, n-1)$, a total of $(n-1)$ equations are found. The n^{th} equation is provided by (4.22b). We obtain

$$\begin{aligned} L_{ao} c f_i = {} & F_{oi}(q_{uoi} q_{\varphi i} - \overline{q_{uo} q_{\varphi}}) \sum_{j=1}^{n-1} f_j(\phi_j - \phi_n) \\ & + F_{oi}(q_{uoi} q_{\sigma i} - \overline{q_{uo} q_{\sigma}}) \frac{1}{2\sigma_0} \sum_{j=1}^{n-1} f_j \left[(\phi_j - \phi_{go})^2 - (\phi_n - \phi_{go})^2\right] \\ & + F_{oi}(q_{uoi} q_{ei} - \overline{q_{uo} q_e})\hat{e} + q_{uoi} f_i - F_{oi} \sum_{j=1}^{n-1} (q_{uoj} - q_{uon}) f_j, \end{aligned} \tag{4.30}$$

$$c\hat{e} = \overline{q_{uo}q_\varphi}\sum_{j=1}^{n-1} f_j(\phi_j - \phi_n) + \overline{q_{uo}q_\sigma}\frac{1}{2\sigma_0}\sum_{j=1}^{n-1} f_j\left[(\phi_j - \phi_{go})^2 - (\phi_n - \phi_{go})^2\right]$$

$$+\overline{q_{uo}q_e}\hat{e} + \sum_{j=1}^{n-1} f_j(q_{uoj} - q_{uon}), \tag{4.31}$$

whence the following linear algebraic eigenvalue problem arises:

$$\boldsymbol{M}\boldsymbol{X} - L_{ao}c\boldsymbol{I} = 0, \tag{4.32}$$

where

$$\boldsymbol{X} \equiv \begin{pmatrix} f_1 \\ f_2 \\ \vdots \\ f_{n-1} \\ \hat{e} \end{pmatrix},$$

and $\boldsymbol{M}$ is the matrix $(i, j = 1, 2, \ldots, n-1)$

$$M_{ij} = \delta_{ij}q_{uoi} + F_{oi}(q_{uoi}q_{\varphi i} - \overline{q_{uo}q_\varphi})(\phi_j - \phi_n) \tag{4.33a}$$

$$+F_{oi}(q_{uoi}q_{\sigma i} - \overline{q_{uo}q_\sigma})\frac{1}{2\sigma_0}\left[(\phi_j - \phi_{go})^2 - (\phi_n - \phi_{go})^2\right] - F_{oi}(q_{uoj} - q_{uon}),$$

$$M_{in} = F_{oi}(q_{uoi}q_{ei} - \overline{q_{uo}q_e}), \tag{4.33b}$$

$$M_{nj} = L_{ao}\left\{\overline{q_{uo}q_\varphi}(\phi_j - \phi_n) + \overline{q_{uo}q_\sigma}\frac{1}{2\sigma_0}\left[(\phi_j - \phi_{go})^2 - (\phi_n - \phi_{go})^2\right]\right\}$$

$$+L_{ao}(q_{uoj} - q_{uon}), \tag{4.33c}$$

$$M_{nn} = L_{ao}\overline{q_{uo}q_e}. \tag{4.33d}$$

The solvability condition for the linear homogeneous algebraic system (4.32) provides the eigenrelationship for our stability problem. In general n eigenvalues for c can be readily obtained from (4.32).

5. The case of weak sorting

In order to clarify the mechanism of bedload sheet instability it is convenient at this stage to consider first the case when sorting is constrained to be 'weak' by the condition of small standard deviation of the base mode. This can be obtained by assuming that the basic density function $F_0(\phi)$ takes the form

$$F_0 = \frac{1}{\sigma_0}F_{00}(\psi), \tag{5.1}$$

where

$$\psi = \frac{\phi - \phi_{go}}{\sigma_0}, \tag{5.2}$$

and

$$\sigma_0 \ll 1. \tag{5.3}$$

The implication is that $F_0(\phi)$ differs only weakly from a Dirac function centred at ϕ_{go}.

The integral conditions (4.13*a*), (4.3*a*,*b*) then lead to the following condition for $F_{00}(\psi)$:

$$\int_{-\infty}^{\infty} F_{00}(\psi)\mathrm{d}\psi = 1, \tag{5.4}$$

$$\int_{-\infty}^{\infty} \psi F_{00}(\psi)\mathrm{d}\psi = 0, \tag{5.5}$$

$$\int_{-\infty}^{\infty} \psi^2 F_{00}(\psi)\mathrm{d}\psi = 1. \tag{5.6}$$

Similarly we may expand $\mathscr{F}(\phi, t)$ in the form

$$\mathscr{F} = \frac{1}{\sigma_0}\left[\mathscr{F}_0(\psi, t) + \sigma_0\mathscr{F}_1(\psi, t) + \sigma_0^2\mathscr{F}_2(\psi, t) + O(\sigma_0^3)\right]. \tag{5.7}$$

Hence, from (4.4):

$$\varphi_g = \sigma_0\varphi_{g1} + O(\sigma_0^2), \qquad \sigma_1 = \sigma_{10} + O(\sigma_0), \tag{5.8a,b}$$

where

$$\varphi_{g1} = \int_{-\infty}^{\infty} \psi\mathscr{F}_0(\psi)\mathrm{d}\psi, \qquad \sigma_{10} = \frac{1}{2}\int_{-\infty}^{\infty} \psi^2\mathscr{F}_0(\psi)\mathrm{d}\psi. \tag{5.9a,b}$$

Furthermore

$$L_{ao} = L_{aoo}[1 + \sigma_0 L_{ao1} + \sigma_0^2 L_{ao2} + O(\sigma_0^3)], \tag{5.10}$$

where

$$L_{aoo} = n_a, \qquad L_{ao1} = \ln 2, \qquad L_{ao2} = (\ln 2)^2. \tag{5.11a–c}$$

The first distinct feature of the bedload sheet mode is the fact that perturbations of bottom amplitude e are passively driven by perturbations of the grain size distribution, being needed only to balance the longitudinal variation of total transport associated with non-uniformity of the grain size distribution. In other words the bedload sheet mode may be characterized by the following expansion for e:

$$e = e_1\sigma_0 + O(\sigma_0^2). \tag{5.12}$$

The latter assumption rules out the 'dune' mode from the output of the present analysis. In fact the appropriate expansion for e in the dune case involves a dominant $O(1)$ contribution corresponding to the development of dunes in uniform sediments. The latter is slightly corrected at higher order in σ_0 by the effects of sorting. We choose not to examine the dune mode here, and rather proceed from (5.12) in our investigation of the bedload sheet mode.

Expanding all the quantities that appear in the integro-differential system (4.22) in powers of σ_0 and collecting terms of the same order, we find a set of linear integro-differential systems that can readily be solved in cascade. Since the algebra involved in this process is rather tedious, we have moved the solution of the systems to Appendix B and discuss here only the structure of the solution itself.

Recalling (5.7) and (5.12) we find

$$\mathscr{F}_0 = f_0(\psi)\exp[-\mathrm{i}\alpha c_0(t + c_1\tau_1 + c_2\tau_2)], \tag{5.13}$$

$$\mathscr{F}_1 = 0 \tag{5.14}$$

$$e_1 = \hat{e}_1\exp[-\mathrm{i}\alpha c_0(t + c_1\tau_1 + c_2\tau_2)], \tag{5.15}$$

where τ_1 and τ_2 are 'slow' time variables, defined in the form

$$\tau_1 = \sigma_0 t, \qquad \tau_2 = \sigma_0^2 t. \tag{5.16a,b}$$

The complex growth rate of perturbations is then found to be

$$c = c_0[1 + \sigma_0 c_1 + \sigma_0^2 c_2 + O(\sigma_0^3)], \tag{5.17}$$

where c_0, c_1 and c_2 follow from the solution of the integro-differential system (4.22) at the various orders of approximation.

It turns out that c_0 and c_1 are real positive numbers, while c_2 is complex. This result clearly displays the second fundamental feature of the bedload sheet mode, namely the fact that it is dominantly a 'sorting wave' which propagates downstream with vanishing growth rate. Growth of the perturbations is seen to arise only at second order.

The amplitude of bottom perturbation $\hat{e}_1$ is given in Appendix B. It should be noticed that $\hat{e}_1$ involves the quantities t_φ, t_σ and t_e, which are complex in general. It hence follows that perturbations of bottom elevation driven by sorting are not in phase with perturbations of the grain size distribution.

In order to clarify the mechanism controlling the formation of bedload sheets, it is particularly instructive to consider first the case of a mixture characterized by a bimodal distribution with small standard deviation modelled as a mixture composed of two sizes, say ϕ_1 and ϕ_2 with $\phi_1 < \phi_2$. Then

$$F_{00} = F_{001}\delta(\phi - \phi_1) + F_{002}\delta(\phi - \phi_2), \tag{5.18}$$

with

$$F_{002} = 1 - F_{001}. \tag{5.19}$$

Hence from (4.3), (5.2) we obtain

$$\phi_{go} = F_{001}(\phi_1 - \phi_2) + \phi_2, \qquad \sigma_0^2 = F_{001}F_{002}(\phi_1 - \phi_2)^2, \tag{5.20a,b}$$

$$\psi_1 = -\left(\frac{F_{002}}{F_{001}}\right)^{1/2}, \qquad \psi_2 = \left(\frac{F_{001}}{F_{002}}\right)^{1/2}. \tag{5.21a,b}$$

Furthermore we may write

$$f_0 = f_{01}\delta(\phi - \phi_1) + f_{02}\delta(\phi - \phi_2), \tag{5.22}$$

with

$$f_{02} = -f_{01}. \tag{5.23}$$

From (B18), (B21), (B25), (B27) (see Appendix B) one finds:

$$c_0 = \frac{q_{uoo}}{L_{aoo}}, \tag{5.24}$$

$$c_1 = -L_{ao1} + \gamma_{10} + \gamma_{11}(F_{002}\psi_1 + F_{001}\psi_2), \tag{5.25}$$

$$\hat{e}_1 = \frac{L_{aoo}}{1 - L_{aoo}q_{eo}}\left[(q_{\varphi o} + \gamma_{11})(\psi_1 - \psi_2) + q_{\sigma o}\tfrac{1}{2}(\psi_1^2 - \psi_2^2)\right] f_{01}, \tag{5.26}$$

$$\begin{aligned} c_2 = {} & -L_{ao2} - L_{ao1}c_1 + \gamma_{20} + \gamma_{21}\psi_1 + \gamma_{22}\psi_1^2 \\ & - F_{001}\left[(\nu_{10} + \nu_{11}\psi_1)(\psi_1 - \psi_2) + (\nu_{20} + \nu_{21}\psi_1)(\psi_1^2 - \psi_2^2)\right]. \end{aligned} \tag{5.27}$$

As mentioned above, c_0 and c_1 are real quantities, which implies that bedload sheets are pure sorting waves up to order σ_0. Growth occurs at order σ_0^2. Let us examine the various contributions displayed by (5.27).

Assume first that $F_{001} = F_{002} = 1/2$, hence $\psi_2 = -\psi_1 = 1$, and neglect the effect of perturbation of bottom elevation on bottom stress. The latter condition will be

seen to arise when the average relative roughness D_{go} is fairly small. Under these conditions (5.27) gives only one contribution to the growth rate, namely

$$\mathrm{Im}(c_2) = \left[F_{001}\Gamma_0\beta \ln 2 \left(\tfrac{5}{2} + \Gamma_s\right) \psi_1 (\psi_1 - \psi_2)\right] \mathrm{Im}(t_\varphi). \tag{5.28}$$

Since the quantities $\Gamma_0, (5/2+\Gamma_s)$ and $[\psi_1(\psi_1-\psi_2)]$ are all invariably positive (5.28) predicts instability provided $\mathrm{Im}(t_\varphi)$ is positive. This finding has a simple physical explanation. Let us consider a flat bed with spatially periodic roughness associated with spatial variations of the fractional content of the two sizes ϕ_1 and ϕ_2. Let us place ourselves at the peak of concentration of the coarser fraction ϕ_1. The growth rate of perturbation is then controlled by the sign of $\partial\mathscr{F}/\partial t$ evaluated at this location. It is straightforward to show that the only contribution to $\partial\mathscr{F}/\partial t$ comes from the quantity

$$-\left[\frac{\partial G}{\partial x} - \int F_0 \frac{\partial G}{\partial x} \mathrm{d}\phi\right]. \tag{5.29}$$

In other words the growth of perturbation of the fractional content of each size is associated with the excess of spatial gradient of transport capacity of that size relative to the average spatial gradient of transport capacity. Now G is an increasing function of ζ and variation in ζ is proportional to variation of τ_{*g} (i.e. to $t_\varphi\varphi_g$). Since the imaginary part of t_φ is positive, the peak of transport capacity for each size fraction is located within the half-wavelength downstream of the peak of coarse sediment. Hence $(-\partial G/\partial x)$ is negative at the peak. Now, if β were identically zero (i.e. the condition of equal mobility of surface material) the quantity $(-\partial G/\partial x)$ would not be a function of ϕ and no growth would arise. The fact that the finer fraction is slightly more mobile renders the quantity $(-\partial G/\partial x)$ slightly larger than the average for the coarser fraction, resulting in growth of the perturbation.

If the condition $F_{001} = F_{002} = 1/2$ is relaxed a second contribution to $\mathrm{Im}(c_2)$ arises:

$$\left[F_{001}\Gamma_0\beta \ln 2 \left(\tfrac{5}{2} + \Gamma_s\right) \psi_1 (\psi_1 - \psi_2)\right] \tfrac{1}{2}(\psi_1 + \psi_2)\mathrm{Im}(t_\sigma) \tag{5.30}$$

Since $t_\sigma = -t_\varphi$ one readily concludes that the effect of the perturbation of the standard deviation on the growth rate is destabilizing provided that the finer fraction is in excess.

Finally if the effect of the bottom elevation perturbation is not negligible, the above conclusions are significantly altered, as noted below.

In order to appreciate the significance of the above discussion it is necessary to point out that the condition $\mathrm{Im}(t_\varphi) > 0$ is satisfied within a region of the (Fr, α)-plane which is quite close to the region where $\mathrm{Im}(t_e) < 0$. The latter condition defines the region where dunes in uniform sediment do not grow. Hence under the assumptions which lead to (5.28), the existence of bedload sheets is predicted only under conditions where dunes are not present. If the effect of t_e is not negligible, however, the regions of existence of dunes and bedload sheets are no longer disjoint.

6. Results and discussion

Before proceeding to a comparison between our theoretical predictions and the observations of Whiting *et al.* (1988) and Kuhnle & Southard (1988) (hereafter referred to as W and K&S respectively), let us substantiate the analysis developed in §5 for the case of mixtures characterized by small standard deviations by comparing the approximate solution for the weak sorting case with the complete solution for arbitrary σ_0 formulated in §4.

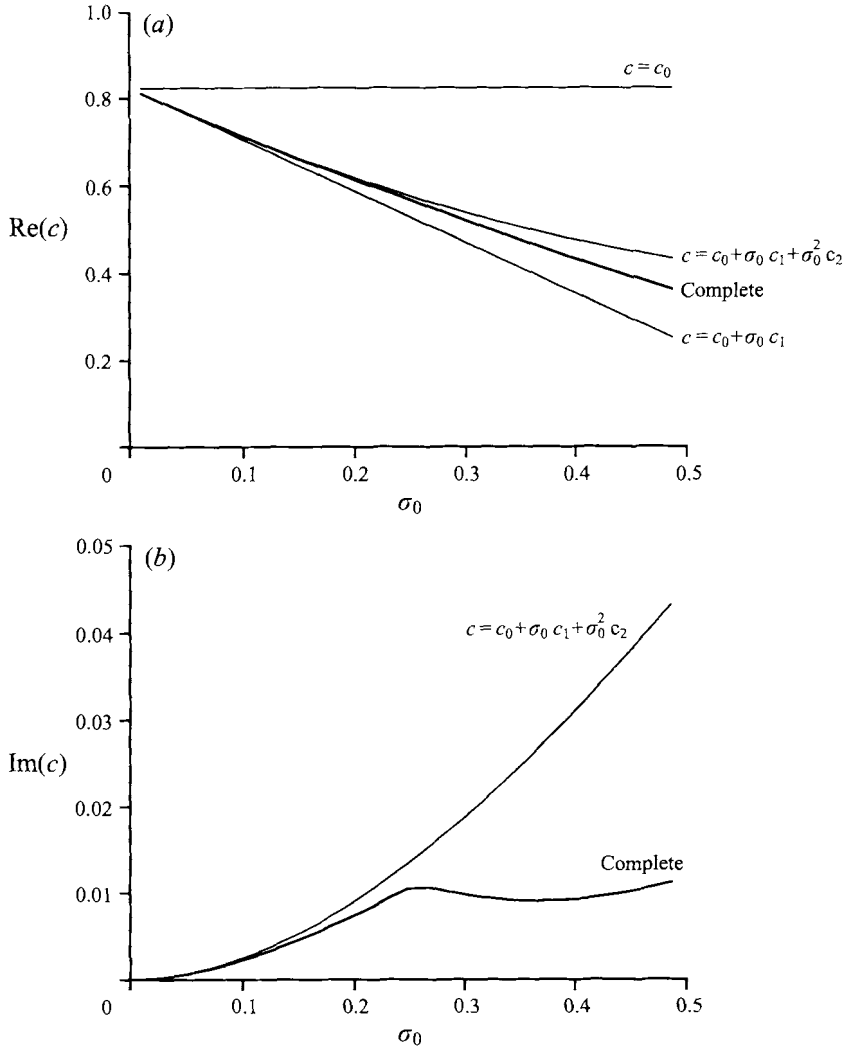

FIGURE 4. (*a*) Real and (*b*) imaginary parts of the growth rate c at various orders of approximation for the weak sorting case and for the solution for arbitrary σ_0

For the sake of simplicity we will consider the case of a mixture composed of equal percentages of two sizes ϕ_1 and ϕ_2.

Figure 4 shows the behaviour of the power series solutions (5.17) for Re(c) and Im(c) at the various orders of approximation and the corresponding complete solution as a function of σ_0 for a given set of parameter values ($\tau_{*go} = 0.065, \alpha = 3, D_{go} = 0.01$). The agreement is quite satisfactory up to a value of σ_0 near 0.25.

We now proceed to compare our predictions with the experimental observations of W and K&S. Whiting *et al.* (1988) observed bedload sheets at Muddy Creek and Duck Creek. The grain size probability density functions for the two creeks are available from W's data. In Muddy Creek the bed was composed of a mixture containing fine and coarse sand while in Duck Creek the bed was a mixture of fine and coarse gravel.

In order to reduce the numerical effort as much as possible we modelled W's

Run	ϕ_1	ϕ_2	ϕ_3	ϕ_4	F_{01}	F_{02}	F_{03}	F_{04}	D_{go}	F_r	τ_{*go}	α
MC	1.5	0.5	−0.5	−1.5	0.24	0.38	0.25	0.13	0.004	0.43	0.135	~ 3.5
DC	1	−1	−2.5	−3.5	0.14	0.25	0.49	0.12	0.013	0.35	0.04	~ 2.5

TABLE 1. Surface grain size distribution and relevant flow and sediment parameters reconstructed from Whiting *et al.* (1988). The mixture is modelled as composed of four grain sizes. MC denotes Muddy Creek and DC Duck Creek.

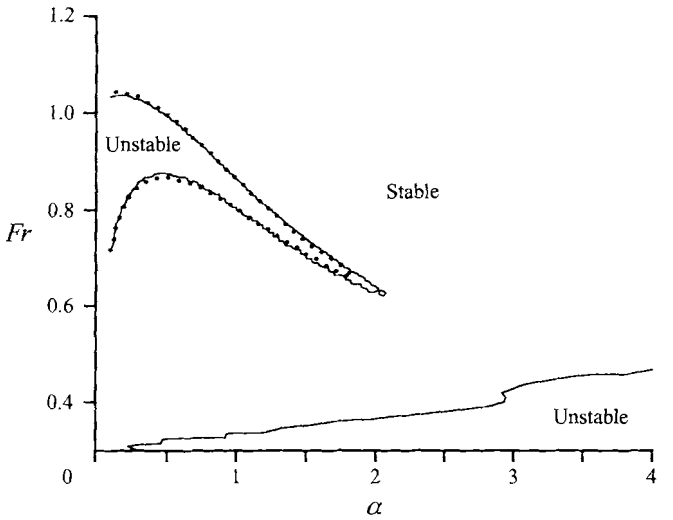

FIGURE 5. Marginal stability curve (solid line) calculated for the values of flow and sediment parameters reconstructed from data reported by Whiting *et al.* (1988) for Muddy Creek. The marginal stability curve obtained on neglecting the effect of bottom elevation on bottom stress is also plotted (dotted line).

mixtures using four sizes, allowing us to derive the eigenrelationship analytically as a solution of a quartic, a task which can also be accomplished analytically.

The values of ϕ_j and $F_{oj}(j = 1,2,3,4)$ reconstructed from the cumulative distributions given in figure 2 of W are reported in table 1, which shows also the flow and sediment parameters reconstructed from W's data.

We then proceeded to determine the stability characteristics of the flow configurations reconstructed for W's observations modelling the mixture as described above. Using the theory developed in §3 we were able to calculate τ_{*g1} as given by (3.25). To this end we solved the differential system (3.23)–(3.25) numerically using a shooting technique. The value of τ_{*g1} was then fed into (4.8)–(4.11), (4.13), (4.17) so that the elements of the matrix $\boldsymbol{M}$ defined by (4.33) could be calculated and the eigenrelationship (4.32) with $n = 4$ determined for the given values of the flow and sediment parameters. In other words we determined four eigenvalues $c_k(k = 1,2,3,4)$ as functions of Fr and α for each of W's observations, i.e. for a given values of D_{go}. Marginal stability is characterized by the condition $\max[\mathrm{Im}(c_k)] = 0$. The preferential wavelength is associated with the maximum value of $\mathrm{Im}(c_k)$ for any given value of Fr and D_{go}.

Figure 5 shows the marginal stability curve for Muddy Creek. Two unstable regions can be recognized in the plot, the lower one for a range of Froude numbers and wavenumbers close to the observed ones. Also shown (dotted lines) are the marginal stability curves obtained on neglecting the effect of perturbation of bottom elevation

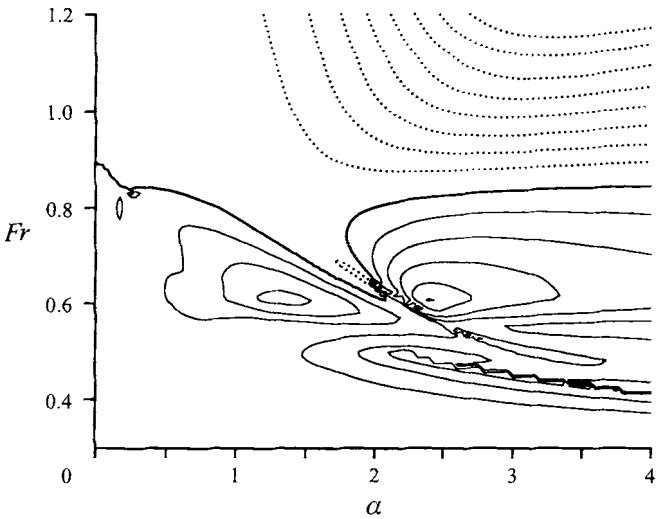

FIGURE 6. Contours of growth rate calculated for the values of flow and sediment parameters reconstructed from data reported by Whiting *et al.* (1988) for Duck Creek. Solid lines and dotted lines represent positive and negative growth rate respectively. The thick solid line is the marginal stability curve.

ϕ_1	ϕ_2	ϕ_3	ϕ_4	F_{01}	F_{02}	F_{03}	F_{04}	D_{go}	Fr
−4.5	−3.5	−1.5	−0.5	0.191	0.496	0.239	0.074	0.1	1.1

TABLE 2. Surface grain size distribution and relevant flow and sediment parameters reconstructed from Kunhle & Southard (1988) (run H3). The mixture is modelled as composed of four grain sizes.

on bottom stress. It turns out that for values of D_{go} as small as for the Muddy Creek case, the latter approximation appears to be justified. Hence the physical mechanism of bedload sheet instability discussed at the beginning of this section for the case of small σ_0 appears to apply to this context. However it should be pointed out that the unstable region in the high-wavenumber range at low Froude numbers does not arise if the effect of t_e is neglected.

As D_{go} increases, as in W's field observations of Duck Creek, the latter approximation is no longer found to be justified. This is shown in figure 6 where the marginal stability curve for Duck Creek is presented. Note that Duck Creek is characterized by a bed composed of fine gravel with $D_{go} = 0.013$, a value nearly four times as large as for Muddy Creek.

It appears that in the case of Duck Creek the unstable region is no longer distinct from that for dunes in uniform sediment (see figure 10 of Richards (1980) for the stability limits for dunes in uniform sediment). However notice that two relative maxima now appear, as opposed to the single maximum associated with dunes in uniform material. As in the case of Muddy Creek, the bedload sheets observed in Duck Creek have wavenumbers within the zone where the theory predicts that they should form.

Comparison with K&S's laboratory observations (run H3) is pursued in figure 7, which shows the marginal stability curves calculated for the values of flow and sediment parameters reconstructed from K&S's data as summarized in table 2.

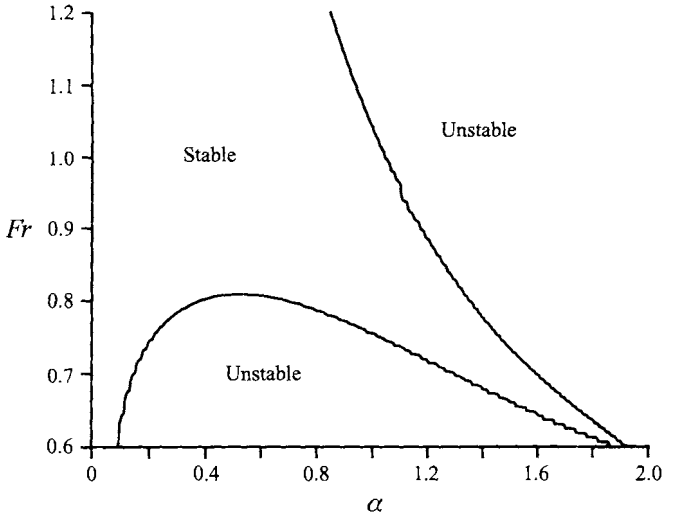

FIGURE 7. Marginal stability curves calculated for the values of flow and sediment parameters reconstructed from data reported by Kuhnle & Southard (1988) (run H3).

Figure 7 suggests that when D_{go} is as large as in K&S's experiments (values of about 0.1, ten times larger than for the Duck Creek observations) the region of instability is no longer clearly distinguishable from that characterizing dune instability, so that the sorting mechanism plays a subsidiary role. Hence under the conditions of K&S's experiments the bedforms could be considered to be either bedload sheets or small-amplitude dunes, the distinction being no longer as clear as for Muddy Creek and Duck Creek.

The authors wish to thank Professor M. Tubino and Professor M. Garcia for interesting discussions in connection with the related problem of dune formation in heterogeneous sediments. This research was partially supported by the Italian Ministero della Ricerca Scientifica e Tecnologica (grant MURST 40% "Trasporto solido") and by the US National Science Foundation (grant no CTS 9207882).

Appendix A

The linear differential operator $\mathbf{L}$ and the matrix $\boldsymbol{A}$ read

$$\mathbf{L} = \begin{pmatrix} l_{11} & l_{12} & l_{13} \\ l_{21} & l_{22} & l_{23} \\ l_{31} & l_{32} & l_{33} \end{pmatrix}, \qquad \boldsymbol{A} = \begin{pmatrix} a_{11} & a_{12} & a_{13} \\ a_{21} & a_{22} & a_{23} \\ a_{31} & a_{32} & a_{33} \end{pmatrix} \tag{A 1}$$

where the coefficients are, respectively,

$$\left.\begin{aligned} l_{11} &= 2\frac{\mathrm{d}}{\mathrm{d}\chi}(v_{T0}\frac{\mathrm{d}}{\mathrm{d}\chi}) - C_0, & l_{12} &= -\frac{\mathrm{d}C_0}{\mathrm{d}\chi} & l_{13} &= \alpha^2, \\ l_{21} &= 2\frac{\mathrm{d}v_{T0}}{\mathrm{d}\chi}, & l_{22} &= \frac{\mathrm{d}C_0}{\mathrm{d}\chi} & l_{23} &= \frac{\mathrm{d}}{\mathrm{d}\chi}, \\ l_{31} &= 1, & l_{32} &= \frac{\mathrm{d}}{\mathrm{d}\chi} & l_{33} &= 0, \end{aligned}\right\} \tag{A 2}$$

with $C_0 = \mathrm{i}\alpha U_0 + \alpha^2 \nu_{T0}$, and

$$\left.\begin{aligned} a_{11} &= -3 + 2\frac{\chi}{R_0+\chi} - (1-\chi)\left[\alpha^2\chi + 2\frac{R_0}{(R_0+\chi)^2}\right], \quad a_{12} = -\alpha^2(1-\chi), \\ a_{13} &= 2\frac{R_0}{R_0+\chi} - (1-\chi)\left[\alpha^2 R_0 - 2\frac{R_0}{(R_0+\chi)^2}\right], \\ a_{21} &= -\chi + 2(1-\chi)\frac{\chi}{R_0+\chi}, \quad a_{22} = -1, \quad a_{23} = -R_0 + 2(1-\chi)\frac{R_0}{R_0+\chi}, \\ a_{31} &= \chi\frac{\mathrm{d}U_0}{\mathrm{d}\chi}, \quad a_{32} = \frac{\mathrm{d}U_0}{\mathrm{d}\chi}, \quad a_{33} = R_0\frac{\mathrm{d}U_0}{\mathrm{d}\chi}. \end{aligned}\right\} \tag{A 3}$$

Appendix B

From (4.18), expanding in powers of σ_0, we readily obtain the relation

$$\Gamma = \left[\frac{\zeta}{G(\zeta)}\frac{\mathrm{d}G}{\mathrm{d}\zeta}\right]_{\zeta=\zeta_0} = \Gamma_0 + \sigma_0\Gamma_1, \tag{B 1}$$

with

$$\Gamma_0 = \left[\frac{\zeta}{G(\zeta)}\frac{\mathrm{d}G}{\mathrm{d}\zeta}\right]_{\zeta=\zeta_{00}}, \qquad \Gamma_1 = \Gamma_{10} + \Gamma_{11}\psi, \tag{B 2a,b}$$

$$\Gamma_{10} = \gamma_{10}(1 - \Gamma_0 + \Gamma_s), \qquad \Gamma_{11} = \gamma_{11}(1 - \Gamma_0 + \Gamma_s), \tag{B 3a,b}$$

$$\gamma_{10} = \Gamma_0\omega_{01} = \Gamma_0\left[\frac{\partial\omega}{\partial\sigma}\right]_{T=T_0,\sigma=0}, \qquad \gamma_{11} = \Gamma_0\beta\ln 2, \tag{B 4a,b}$$

and, finally,

$$\zeta_{00} = \frac{\tau_{*go}}{\tau_{*r}}, \qquad \Gamma_s = \left[\zeta\frac{\mathrm{d}^2G}{\mathrm{d}\zeta^2}\frac{\mathrm{d}\zeta}{\mathrm{d}G}\right]_{\zeta=\zeta_{00}}. \tag{B 5a,b}$$

From (4.14) we obtain the expansion

$$q_{uo} = \tau_{*go}^{3/2} G_{00}(1 + \sigma_0 G_{01} + \sigma_0^2 G_{02}) = q_{uoo}(1 + \sigma_0 G_{01} + \sigma_0^2 G_{02}), \tag{B 6}$$

where

$$G_{00} = G(\zeta_{00}), \qquad G_{01} = \gamma_{10} + \gamma_{11}\psi, \qquad G_{02} = \gamma_{20} + \gamma_{21}\psi + \gamma_{22}\psi^2, \tag{B 7a–c}$$

and

$$\gamma_{20} = \gamma_{10}^2\frac{\Gamma_s}{2\Gamma_0}, \quad \gamma_{21} = \gamma_{10}\gamma_{11}\frac{1+\Gamma_s}{\Gamma_0}, \quad \gamma_{22} = \gamma_{11}^2\frac{1+\Gamma_s}{2\Gamma_0}. \tag{B 8a–c}$$

Furthermore the following expansions for q_φ, q_σ and q_e are assumed:

$$(q_\varphi, q_\sigma, q_e) = (q_{\varphi o}, q_{\sigma o}, q_{eo}) + \sigma_0(q_{\varphi 1}, q_{\sigma 1}, q_{e1}) + O(\sigma_0^2), \tag{B 9}$$

where

$$q_{\varphi o} = \left(\tfrac{3}{2} + \Gamma_0\right)t_\varphi + \Gamma_0\ln 2(1-\beta), \quad q_{\sigma o} = \left(\tfrac{3}{2} + \Gamma_0\right)t_\sigma + \Gamma_0\omega_{o1}, \quad q_{eo} = \left(\tfrac{3}{2} + \Gamma_0\right)t_e, \tag{B 10a–c}$$

and

$$(q_{\varphi 1}, q_{\sigma 1}, q_{e1}) = (q_{\varphi 1}^0, q_{\sigma 1}^0, q_{e1}^0) + \psi(q_{\varphi 1}^1, q_{\sigma 1}^1, q_{e1}^1). \tag{B 11}$$

In the above relations

$$q^0_{\varphi 1} = \Gamma_{10}\left[\ln 2(1-\beta) + t_\varphi\right] + \Gamma_0\omega_{T1}(\ln 2 + t_\varphi), \quad q^1_{\varphi 1} = \Gamma_{11}\left[\ln 2(1-\beta) + t_\varphi\right], \tag{B 12a,b}$$

$$q^0_{\sigma 1} = \Gamma_{10}(t_\sigma + \omega_{01}) + \Gamma_0\omega_{T1}t_\sigma, \qquad q^1_{\sigma 1} = \Gamma_{11}(t_\sigma + \omega_{01}), \tag{B 13a,b}$$

$$q^0_{e1} = (\Gamma_{10} + \Gamma_0\omega_{T1})t_e, \qquad q^1_{e1} = \Gamma_{11}t_e, \tag{B 14a,b}$$

and, finally,

$$\omega_{T1} = \left[T\frac{\partial^2\omega}{\partial T\partial\sigma}\right]_{T=T_0,\sigma=0} \tag{B 15}$$

We can now proceed to solve the integro-differential system (4.22) at the various orders of approximation.

$O(\sigma_0^{-1})$

At $O(\sigma_0^{-1})$ (4.21) gives

$$L_{aoo}\mathscr{F}_{o,t} + \mathrm{i}\alpha q_{uoo}\mathscr{F}_0 = 0, \tag{B 16}$$

an equation which is readily solved in the form

$$\mathscr{F}_0 = f_0(\psi)\exp(-\mathrm{i}\alpha c_0 t)E_1(\tau_1)E_2(\tau_2), \tag{B 17}$$

where

$$c_0 = \frac{q_{uoo}}{L_{aoo}}. \tag{B 18}$$

$O(\sigma_0^0)$

Proceeding to the next approximation, we find from (4.22*a*)

$$L_{aoo}\mathscr{F}_{1,t} + \mathrm{i}\alpha q_{uoo}\mathscr{F}_1 = - L_{aoo}L_{ao1}\mathscr{F}_{o,t} - L_{aoo}\mathscr{F}_{o,\tau_1} - \mathrm{i}\alpha q_{uoo}\left(G_{01}\mathscr{F}_0 - F_{00}\int_{-\infty}^{\infty} G_{01}\mathscr{F}_0\,\mathrm{d}\psi\right). \tag{B 19}$$

Equation (B 19) is readily solved setting

$$E_1 = \exp(-\mathrm{i}\alpha c_0 c_1 \tau_1), \tag{B 20}$$

in (B 17), with c_1 specified by the integral equation

$$c_1 f_0 + L_{ao1}f_0 - G_{01}f_0 - F_{00}\gamma_{11}\int_{-\infty}^{\infty}\psi f_0\,\mathrm{d}\psi = 0. \tag{B 21}$$

Furthermore we can now set

$$\mathscr{F}_1 \equiv 0, \tag{B 22}$$

as (B 20) and (B 21) reduce (B 19) to a homogeneous equation for $\mathscr{F}_1$ identical with (B 16), allowing its solution to be absorbed into $\mathscr{F}_0$.

The amplitude e_1 of the bottom perturbation driven by the sorting wave satisfies the equation obtained from (4.22*b*) at $O(\sigma_0)$, which reads

$$e_{1,t} = \mathrm{i}\alpha q_{uoo}\left[(q_{\varphi o} + \gamma_{11})\int_{-\infty}^{\infty}\psi\mathscr{F}_0\,\mathrm{d}\psi + q_{\sigma o}\frac{1}{2}\int_{-\infty}^{\infty}\psi^2\mathscr{F}_0\,\mathrm{d}\psi + q_{eo}e_1\right]. \tag{B 23}$$

Hence the solution for e_1 is

$$e_1 = \hat{e}_1 \exp(-\mathrm{i}\alpha c_0 t) E_1(\tau_1) E_2(\tau_2), \tag{B 24}$$

where

$$\hat{e}_1 = \frac{L_{aoo}}{1 - L_{aoo} q_{eo}} \left[(q_{\varphi o} + \gamma_{11}) \int_{-\infty}^{\infty} \psi f_0 \mathrm{d}\psi + q_{\sigma o} \frac{1}{2} \int_{-\infty}^{\infty} \psi^2 \hat{f}_0 \mathrm{d}\psi \right]. \tag{B 25}$$

$O(\sigma_0)$

Proceeding to the next order we find from (4.22*a*):

$$\begin{aligned} L_{aoo}\mathscr{F}_{2,t} + \mathrm{i}\alpha q_{uoo}\mathscr{F}_2 = & -L_{aoo}L_{ao2}\mathscr{F}_{o,t} - L_{aoo}L_{ao1}\mathscr{F}_{o,\tau_1} - L_{aoo}\mathscr{F}_{o,\tau_2} \\ & - \mathrm{i}\alpha q_{uoo} F_{00} \left\{ \left[(q_{\varphi 1} + q_{\varphi o} G_{01}) - \overline{(q_{\varphi 1} + q_{\varphi o} G_{01})} \right] \varphi_{g1} \right. \\ & \left. + \left[(q_{\sigma 1} + q_{\sigma o} G_{01}) - \overline{(q_{\sigma 1} + q_{\sigma o} G_{01})} \right] \sigma_{10} + \left[(q_{e1} + q_{eo} G_{01}) - \overline{(q_{e1} + q_{eo} G_{01})} \right] e_1 \right\} \\ & - \mathrm{i}\alpha q_{uoo} \left(G_{02}\mathscr{F}_0 - F_{00} \int_{-\infty}^{\infty} G_{02}\mathscr{F}_0 \mathrm{d}\psi \right), \end{aligned} \tag{B 26}$$

where the overbar is defined by (4.23) with F_{00} instead of F_0.

The solvability condition is readily found to read

$$\begin{aligned} & [L_{ao2} + L_{ao1} c_1 + c_2 - G_{02}] f_0 \\ & \quad + F_{00} \left[(\nu_{10} + \nu_{11}\psi) \int_{-\infty}^{\infty} \psi f_0 \mathrm{d}\psi + (\nu_{20} + \nu_{21}\psi) \int_{-\infty}^{\infty} \psi^2 f_0 \mathrm{d}\psi \right] = 0, \end{aligned} \tag{B 27}$$

having set

$$E_2 = \exp(-\mathrm{i}\alpha c_0 c_2 \tau_2), \tag{B 28}$$

and

$$\nu_{10} = \gamma_{21}, \tag{B 29}$$

$$\nu_{11} = -\left[\frac{L_{aoo}}{1 - L_{aoo} q_{eo}} (q_{\varphi o} + \gamma_{11})(q^1_{e1} + q_{eo}\gamma_{11}) + (q^1_{\varphi 1} + q_{\varphi o}\gamma_{11}) \right], \tag{B 30}$$

$$\nu_{20} = \gamma_{22}, \tag{B 31}$$

$$\nu_{21} = -\frac{1}{2} \left[\frac{L_{aoo}}{1 - L_{aoo} q_{eo}} q_{\sigma o} (q^1_{e1} + q_{eo}\gamma_{11}) + (q^1_{\sigma 1} + q_{\sigma o}\gamma_{11}) \right]. \tag{B 32}$$

REFERENCES

ANTONIA, R. A. & LUXTON, R. E. 1971 The response of a turbulent boundary to a step change in surface roughness. Part 1. *J. Fluid Mech.* **48**, 721–761.

ANTONIA, R. A. & LUXTON, R. E. 1972 The response of a turbulent boundary to a step change in surface roughness. Part 2. *J. Fluid Mech.* **49**, 737–757.

ASHIDA, K. & MICHIUE, M. 1972 Study on hydraulic resistance and bedload transport rate in alluvial streams. *Trans. JSCE* **206**, 59–69.

EGIAZAROFF, I. V. 1965 Calculation of nonuniform sediment concentrations. *J. Hydraul. Div. ASCE* **91** HY4, 225–247.

EINSTEIN, H. A 1950 The bed-load function for sediment transportation in open channel flows. *Tech. Bull.* 1026, USDA Soil Conservation Service.

ENGELUND, J. F. & FREDSØE, J. 1982 Sediment ripples and dunes. *Ann. Rev. Fluid Mech.* **14**, 13–37.

HIRANO, M. 1971 River bed degradation with armoring. *Trans. JSCE* **195**, 55–65.

ISEYA, F. & IKEDA, H. 1987 Pulsations in bedload transport rate induced by a longitudinal sediment sorting: a flume study using sand and gravel mixtures. *Geografiska Annaler* **69** A(1), 15–27.

JACOBS, W. 1939 Umformung eines turbulenzen Geschwindigkeits-Profils. *Z. Angew. Math. Mech.* **19**, 87–100 (quoted from *Boundary-Layer Theory* by H. Schlichting, 6th edn., pp. 615–616, McGraw-Hill, 1968).

KENNEDY, J. F. 1963 The mechanics of dunes and antidunes in erodible-bed channels. *J. Fluid Mech.* **16**, 521–544.

KUHNLE, R. A. & SOUTHARD, J. B. 1988 Bed load transport fluctuations in a gravel bed laboratory channel. *Water Resources Res.* **24**. 247–260.

NAKAGAWA, H. & TSUJIMOTO, T. 1980 Sand bed instability due to bed load motion. *J. Hydraul. Div. ASCE* **106** HY12, 2029–2051.

NEZU, I., NAKAGAWA, H., SEYA, K. & SUZUKI, Y. 1990 Response of velocity profile and bed shear stress to abruptly changed roughness in open-channel flows. *Proc. Hydraul. Engng JSCE* **34**, 505–510 (in Japanese).

PARKER, G. 1990 Surface-based bedload transport relation for gravel rivers. *J. Hydraul. Res.* **20** 4, 417–436.

PARKER, G. 1991 Selective sorting and abrasion of river gravel. I: Theory. *J. Hydraul. Engng ASCE* **117** 2, 131–149.

PARKER, G. 1992 Some random notes on grain sorting. *Proc. Grain Sorting Seminar, Ascona, Switzerland*, pp. 19–76.

PARKER, G. & KLINGEMAN, P. C. 1982 On why gravel-bed streams are paved. *Water Resources Res.* **18** 5, 1409–1423.

PROFFIT, G. T. & SUTHERLAND, A. J. 1983 Transport of non-uniform sediments. *J. Hydraul. Res.* **21** 1, 33–43.

RIBBERINK, J. S. 1987 Mathematical modelling of one-dimensional morphological changes in rivers with non-uniform sediment. PhD thesis, Delft University of Technology.

RICHARDS, K. J. 1980 The formation of ripples and dunes on an erodible bed. *J. Fluid Mech.* **99**, 597–618.

SAMAGA, B. R., RANGA RAJU, K. G. & GARDE, R. J. 1986 Bed load transport of sediment mixtures. *J. Hydraul. Engng ASCE* **112**, 1003–1018.

SEMINARA, G. & TUBINO, M. 1989 Alternate bars and meandering: free, forced and mixed interactions. In *River Meandering* (ed. S.Ikeda & G.Parker). AGU Water Resources Monograph, vol. 12, pp. 267–320.

TOWNSEND, A. A. 1961 Equilibrium layers and wall turbulence. *J. Fluid Mech.* **11**, 97–120.

TOWNSEND, A. A. 1965 The response of a turbulent boundary layer to abrupt change in surface condition. *J. Fluid Mech.* **22**, 799–822.

TSUJIMOTO, T. 1989 Instability of longitudinal distribution of fluvial bed-surface composition. *J. Hydrosci. Hydr. Engng JSCE* **7**, 69–80.

TSUJIMOTO, T., CARDOSO, A. H. & SAITO, A. 1990 Open channel flow with variable bed shear stress. *Proc. Hydraul. Engng JSCE* **34**, 433–438 (in Japanese).

WHITE, W. R. & DAY, T. J. 1982 Transport of graded gravel bed material. In *Gravel-Bed Rivers* (ed. R.D. Hey, J.C. Bathurst & C.R. Thorne), pp. 181–224. John Wiley and Sons.

WHITING, P. J., DIETRICH, W. E., LEOPOLD, L. B. & COLLINS, L. 1985 The variability of sediment transport in a fine gravel stream. *Proc. Intl Fluvial Sedimentalogy Conf. 3rd. Fort Collins*, p. 38. Colorado State Univ. Press.

WHITING, P. J., DIETRICH, W. E., LEOPOLD. L. B., DRAKE, T. G. & SHREVE, R. L. 1988 Bedload sheets in heterogeneous sediment. *Geology* **16**, 105–109.